

Oxide Film Properties on an Interstitial-Free Manganese alloyed Steel in Sodium Sulphate Solution

Hongxing Chen^{1,3}, Jianzhong Li^{2,*}, Pin Du², Zihan Yu², Changsheng Liu¹

¹ School of Materials Science and Engineering, Northeastern University, Shenyang 110819, China;

² School of Metallurgy, Northeastern University, Shenyang 110819, China;

³ Baoshan Iron & Steel CO., LTD., Shanghai 201900, China

*E-mail: lijz@mail.neu.edu.cn

Received: 6 February 2018 / Accepted: 13 March 2018 / Published: 10 April 2018

Components of oxide films on interstitial-free (IF) manganese alloyed steel significantly affect corrosion resistance, and the formation of oxide films and their properties are closely related to the enrichment of alloying elements and the structure of IF manganese alloyed steel. The components and electrochemical properties of oxide films formed on IF manganese alloyed steel were measured by X-ray photoelectron spectroscopy (XPS) and electrochemical tests using 1×10^{-5} mol/L Na_2SO_4 solution as an electrolyte for different annealed samples with Mn content (wt%) from 0.079 to 0.556. The results showed that the corrosion resistance of oxide films generated on IF manganese alloyed steel decreases with Mn enrichment. According to analysis by X-ray diffraction (XRD) and electron backscatter diffraction (EBSD), with augmented Mn content, the crystal-oriented distribution of samples becomes obviously concentrated, and the volume fraction of $\{111\}$ //ND texture increases. It is confirmed the significant role of the Mn content on grain refinement of IF manganese alloyed steel. In addition, the oxides of other elements (Si and Fe) tend to hold steady with increasing Mn content.

Keywords: IF manganese alloyed steel, oxide film, corrosion resistance, texture, grain orientation

1. INTRODUCTION

Given its excellent formability and high strength, as well as excellent surface quality, interstitial-free (IF) steel has been widely used as a sheet material in manufacturing, for instance in stamping parts with intricate shapes for automotive applications and electrical appliances[1]. However, corrosion defects easily appear on IF steel substrate without a galvanized layer, so the corrosion properties of IF steel have great importance for their potential applications[2].

The passive anti-corrosive performance of materials in a multifarious hostile environment primarily derives from the protective film that emerges on the surface. Passive properties are always

classified in a relatively inert situation, which by definition involves the metal playing a relatively sluggish role compared to the role predicted beyond thermodynamic conditions[3]. The complicated passivation process is influenced by various factors: the environment, the circumstances of formation and the alloy composition. Importantly, the alloy elements in steels may alter their corrosive properties on account of differences in their electrochemical performance. Elements like titanium, niobium, phosphorus, manganese and silicon, as minor parts of an alloy, play large roles in the mechanical and electrochemical characteristics of IF steel. Nevertheless, records as far back as the 1950s[4] and recent studies[5] manifested the power of enriching with surface-oxidized alloying elements (such as silicon, manganese and titanium) the surface part of IF steel. To achieve oxidation, such steels are treated with short annealing times under decreasing pressure at 850°C. Data has suggested that the passive behaviour of IF steel surface is related to the formation of a complex oxide film, consisting of a rich iron-oxide outer layer and manganese-oxide with, discontinuously, silicon-oxide, a nitrides layer, other types of precipitates in the inner layer, and so on[6,7].

Ana Paula de Andrade Manfridini et al[8,9] investigated nitrides in the surface of plasma nitride IF steel, finding that the corrosion resistance of the nitride layer depends on the type of nitride formed in the compound layer. Accumulated studies[10-13] have examined the behaviour of FeTiP as precipitate in IF titanium alloyed steel, along with the effects of the grain-boundary character on intergranular corrosion and cyclic deformation. Other earlier reports[14-16] on the corrosion behaviour of carbon steel have shown that quantifying temperature, pH and the existence of ionizing radiation all significantly control the composition of phase, chemical element distribution, morphological behaviour and the thickness of the oxide film which is formed on carbon steel. R. Sánchez Tovar et al[17] evaluated the corrosion resistance of duplex stainless steel to the diverse phases of oxide growth in air using methods at high temperature, such as Raman spectroscopy. They found that the anti-corrosive quality of the superficial substance tends to lower with increases in the amount of oxides (particularly γ -Fe₂O₃ and Fe₃O₄) and heat-treatment temperature. Based on a similar theoretical direction, Xiahe Liu[18] discussed the effects and the electrochemical corrosion properties of a one-element beneficiation of surface-oxide film; specifically, Zn was injected to 304 SS at 573.15K for 48h. With Zn enrichment, the ampere density of the negative pole reduced, and hence the resistance capability of the films increased, while the thickness of the slight oxide substance on the outer plane decreased. Also, the electrochemical performance and corrosive-resistant behaviour of the slight substance on the outer plane that is formed on materials has been previously studied by certain groups in water at 1060°C and 705°C with Zn added at various levels[19,20].

All of these studies have shown that elemental content significantly influences the formation of the outer layer of oxide films and the corrosion rate, making it necessary to study elemental enrichment to understand the layer-sediments and surface-oxide film properties of IF steel. Concerning the performance of IF steel, manganese alloys control the stacking-fault energy and maintain steel's austenitic structure. However, no systematic studies, to our knowledge, have examined the properties of surface-oxide film formed on IF manganese alloyed steel. For this reason, the present experiments detail and evaluate the microscopic structure and texture of IF manganese alloyed steel without any coating or physical protection connected with changing Mn content. The effect of Mn content in IF

manganese alloyed steel on the corrosion resistance of the surface oxide film in sodium sulphate solution, moreover, is analysed.

2. EXPERIMENT

Used for the experiments were self-supplied (from Bao Steel CO., LTD., China) samples of IF manganese alloyed steel with Mn content (wt%) at 0.079, 0.311 and 0.556, respectively. Table 1 summarizes the chemical compositions of the specimens. The substrates were mechanically polished with emery papers up to 1000 grit to ensure similar surface roughness. Three types of the alloys status were conducted as the heating treatment showed in Figure 1. During the experiment, the working gas of nitrogen was introduced into the chamber through a mass flow controller with gradual flow rate increase and a final flow rate of 40 sccm. And then the samples were water-quenched using deionized water at 60 °C.

The compositions of the outer oxide layer of different IF manganese alloyed steel were analysed by ESCALAB250 multifunctional X-ray photoelectron spectrometer (XPS) from Thermo VG. The test conditions were an Al K_α excitation source, target voltage steady at 15 kV, target current of 10 mA, vacuum chamber pressure under 2×10⁻⁶ Pa, measurement step maintained at 0.1eV and sputtering speed held at 0.2 nm/s.

Table 1. Chemical compositions of IF manganese alloyed steel (wt%)

C	Si	Mn	P	S	Nb	Ti	B
		0.079					
0.0019	<0.03	0.311	0.010	0.0052	<0.010	0.068	<0.0001
		0.556					

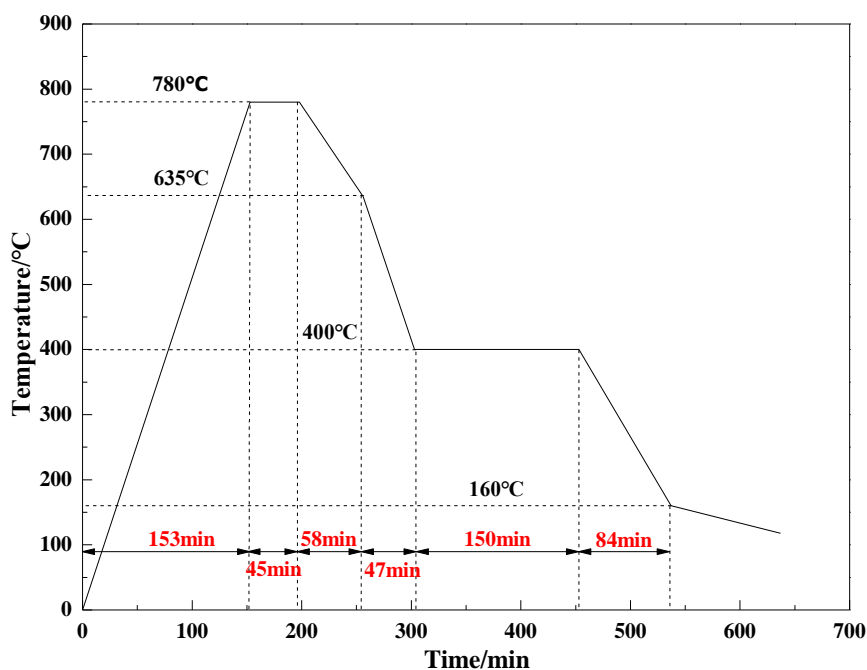


Figure 1. Heating treatment diagram

Electrochemical tests were performed using an RST5200 electrochemical workstation. To ensure stable electrochemical properties for the oxide films on interstitial-free manganese alloyed steel, the electrode was treated with 1.0×10^{-5} mol/L Na_2SO_4 as an electrolyte. The samples were used as the working electrode, graphite was used as the auxiliary electrode and the reference electrode used saturated potassium chloride solution. The sample test area measured $10\text{mm} \times 10\text{mm}$, and the other surfaces were sealed with polytetrafluoroethylene. The test parameters of the Tafel curve were potential range of $-1.2-0$ V and scanning rate at approximately 0.05 mV/s. The AC impedance spectrum test used frequency ranges of $0.01-10^5$ Hz and amplitude at 10mA . The test parameters of the Mott-Schottky plot were potential range $-1.0-0.2$ V and scanning rate of 50 mV/s.

Regarding the EBSD experiment, the IF manganese alloyed steel samples with different Mn content were ground with sandpaper and then polished by argon ion. Next, raw data were collected by means of an EBSD probe configured on a NOVA400Nano-SEM field emission scanning electron microscope (SEM). Then, the original data were processed by the HKL company's Channel software package, capturing the relevant data, such as the orientation difference-function graphs of the sample.

Eventually, the textures during the crystallization of the substrate outer layer were characterized by applying a goniometer connected to the X'pert XRD (x-ray diffraction) machine. For texture analysis, IF manganese alloyed steel samples with different Mn content were placed in 1:100 dilute hydrochloric acid solution for about 2 min, with a Co diffraction target, voltage of 40 kV, current of 40 mA, step $\Delta\alpha=5^\circ$, $\Delta\beta=5^\circ$, scanning range α of $0-70^\circ$ and β of $0-360^\circ$. After processing the data, the polar diagram, the inverse polar diagram and the orientation distribution-function graph were obtained. The (111) and (110) pole pictures were calculated by using the method of Bunge[21] applied in the Labotex software. These pictures were derived from a functional relationship, namely the Orientation Distribution Functions (ODFs).

3. RESULTS AND DISCUSSION

3.1 Effect of Mn content on the oxide composition of IF manganese alloyed steel

Figure 2 shows representative XPS spectra of Fe3p, Mn3p and Si3p from the oxide films on IF manganese alloyed steel with different manganese content. Using the spectra, we searched for constituent parts of the surface films that are inactivated and passive. Sputtering time was chosen as 10s to avoid the influence of surface oxides, which represent a high percentage of defects, including positive ion vacancies, oxygen vacancies, positive ion interstitials and substitutional atoms[22]. The peak values, corresponding to the binding energy, are related to the reference peaks in the Guidebook of X-ray photoelectron spectroscopy[23]. The Fe and Si peaks had typical appearance, but the Fe and Si details showed dominant links with superficial oxide film on the IF manganese alloyed steel, with tiny Mn peaks for the Mn content (wt %) of 0.079 . Mn peaks were obviously detected in the oxide films on the IF manganese alloyed steel for Mn content (wt%) of 0.311 and 0.556 . In the spectra of Fe and Si, the low binding energy peaks (around 706.79 eV for Fe0 or 99.3eV for Si0) changed almost imperceptibly for different Mn content. Additionally, the metallic-state content in the array might also be detected through the thin film.

Concerning the Fe spectrum, the higher energy peaks can be assigned to some form of iron oxide (around 708.875eV for FeO, 708.369eV for Fe₂O₃ or 711.552eV for Fe₃O₄), remaining virtually unchanged with different manganese content. In the Si spectrum, higher binding energy can be ascribed to different valences of silicon oxide (around 101.978eV for SiO or 102.046eV for SiO₂). With increasing manganese content in IF manganese alloyed steel, according to the peak area ratio, SiO content in the oxide film decreased and SiO₂ content increased.

For the Mn spectrum, with increasing manganese content, more obvious Mn peaks were detected in the oxide film, with different valences of manganese oxides (around 640.7eV for MnO, 641.5eV for Mn₂O₃, 642.2eV for MnO₂ or 641.6eV for Mn₃O₄). The percentage of total Mn in the oxide film of IF manganese alloyed steel with Mn content (wt%) of 0.556 was larger than that of Mn content (wt%) at 0.311 and 0.079. Especially for Mn content (wt%) of 0.556, more oxide species with different valences were found. These results demonstrate that an outer Mn-rich layer formed in the oxide films, suggesting that manganese easily migrates from the inner matrix to the outer surface for samples under heat treatment. In addition, the oxides of other elements (Si and Fe) tend to hold steady with increasing Mn content.

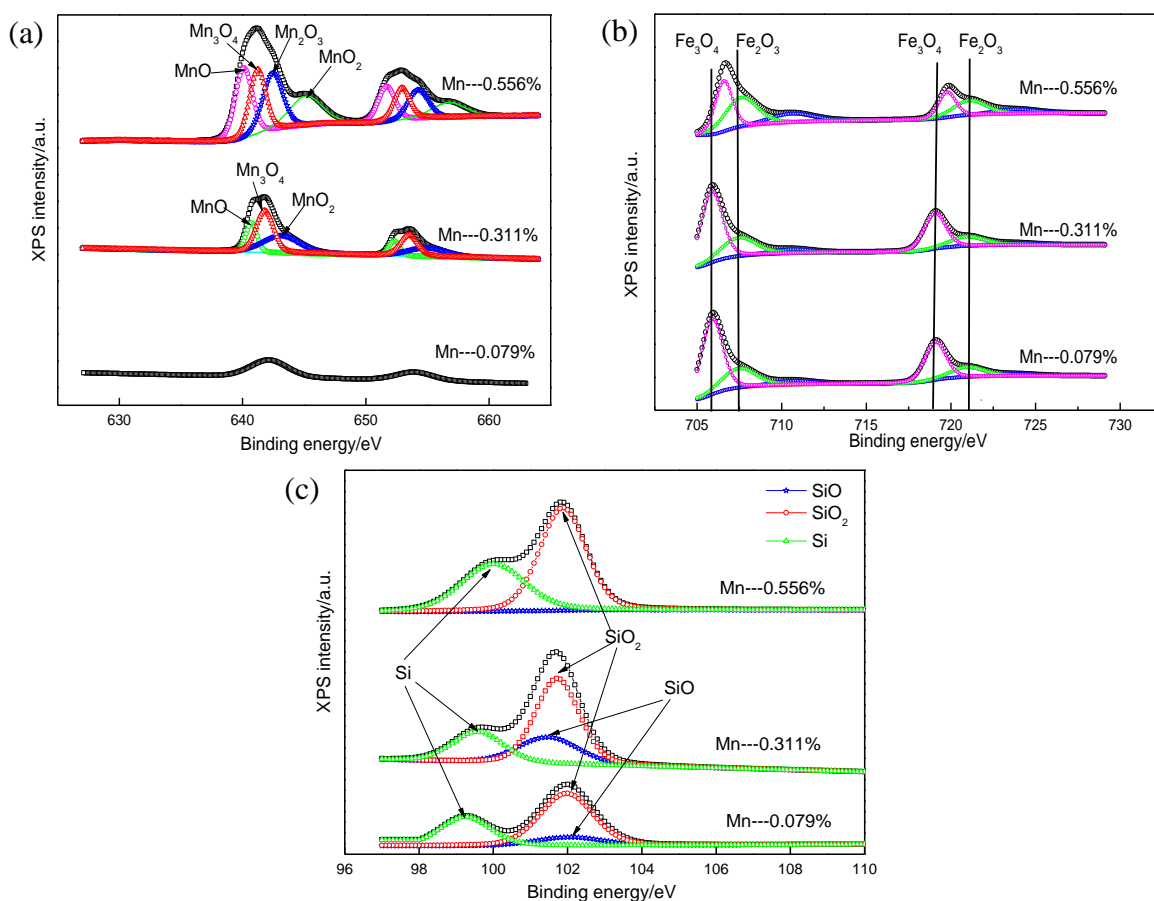


Figure 2. Representative XPS spectra on oxide film of IF manganese alloyed steel with different Mn content: (a) Mn spectra; (b) Fe spectra; (c) Si spectra.

3.2 Electrochemical performances of the oxide film on IF manganese alloyed steel

In order to further evaluate the influence of Mn capacity on the performance of the oxide film on IF manganese alloyed steel, the following electrochemical measuring methods were performed using 1×10^{-5} mol/L Na_2SO_4 solution as an electrolyte: Electrochemical Impedance Spectroscopy (EIS), principles of potentiodynamic polarization and Mott-Schottky curves. Results are shown in Figure 3, and the fitted values of the parameters are listed in Table 2. In Figure 3a, the anodic peak between -0.3V and 0.2V (SHE) for potentiodynamic curves may be related to the passive and protective surface film formation of iron oxide. With more Mn injection, the passive area decreased, vanishing at Mn content (wt%) of 0.556. The corresponding I_{corr} in Table 2 increased with increasing Mn content. Therefore, according to the polarization curves, Mn content induced the oxide film formed on the IF manganese alloyed steel to generate a less protective outer layer. Concerning EIS measurements performed in Na_2SO_4 solution, for three samples, the electrochemical impedance spectra of the Nyquist plots revealed two clearly capacitive arcs, but there was a somewhat unfinished capacitive arc at high frequency (HF) for IF manganese alloyed steel with different Mn content.

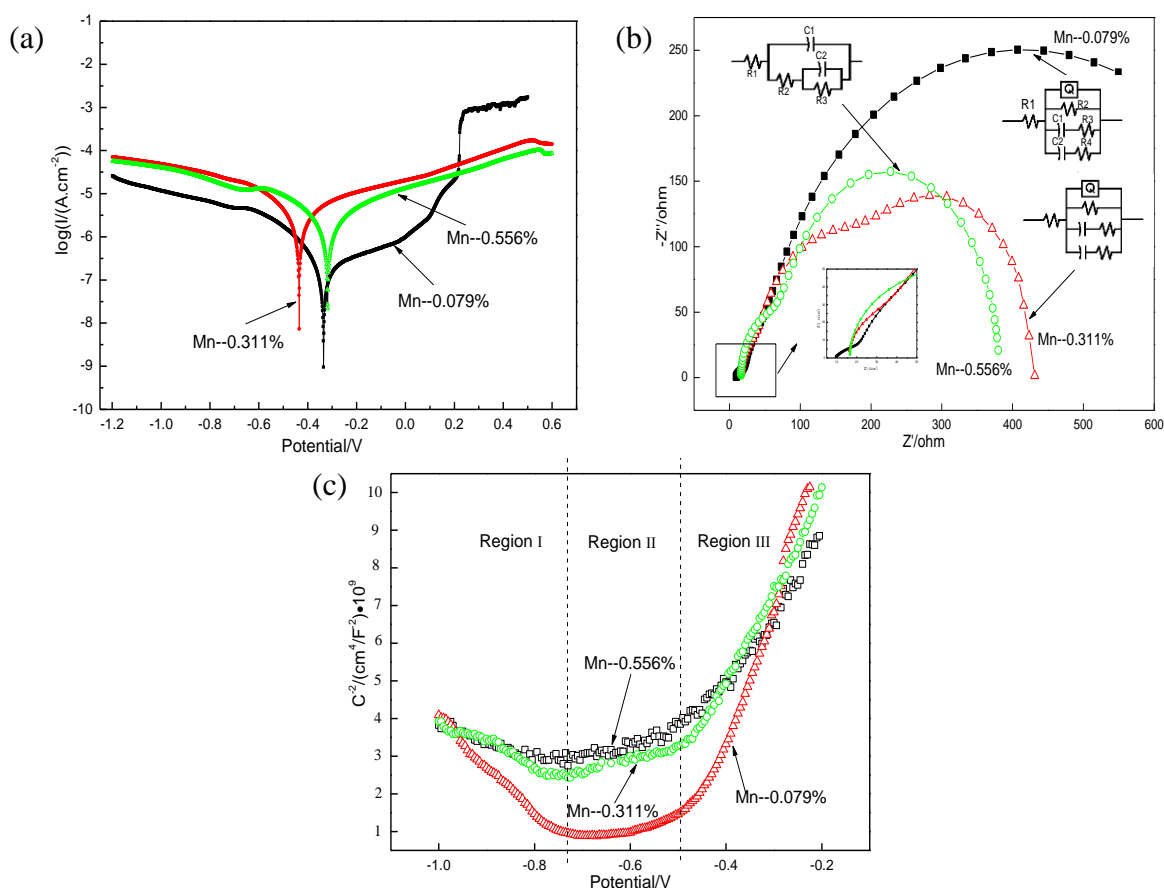


Figure 3. Electrochemical parameters of different types of IF manganese alloyed steel in 1.0×10^{-5} mol/L Na_2SO_4 solution: (a) Potentiodynamic polarization; (b) Impedance Spectroscopy; (c) Mott-Schottky curves.

In addition, with increasing Mn content in IF manganese alloyed steel, the electrochemical capacitance arc radius of the test samples increased at high frequency but decreased at middle frequency (MF) and low frequency (LF), depending on the density of the oxide film, as shown by the sharp decrease in the impedance values. Usually, capacitive bends at HF and MF are attributable to both transfer of charge and the double layer, which is correlated with the space between the electrolyte solution and the IF manganese alloyed steel. As N. Pebere reported [24,25], the capacitive bends are the relaxation of gradually growing mass transmitting inside the solid oxide phase. According to these results, R1 could be connected to the pair layer of Helmholtz and hence to the multi-hole outermost stratum. R1 has a regular, increasing trend with increasing Mn content across the high-frequency range. R2, however, can be considered a dense inner layer, which linearly decreases with increasing Mn content across the middle- and low-frequency range. Other parameters may be related to the properties of oxide film and the electrolyte. A clear trend is observed in the charge transfer resistance, coincident with reduced protection against corrosion as Mn content increases. These results measured the special dependence of the depletion-stratum thickness on potential and are similar to the Mott-Schottky performance shown in Figure 3c.

The barrier layer may have relatively high impedance in the low-frequency arc. Also, the outermost layer, which is a porous, double-layer termed Helmholtz, and the internal layer may have low impedance in the high-frequency arc. The anti-corrosive performance of the thin oxide layer of IF manganese alloyed steel is connected with its semiconducting performance [26], which could be evaluated by the Mott-Schottky analytical method in the high-frequency domain [27]. Corresponding to the Mott-Schottky theories, the space charge capacitance, comprising n-type and p-type semiconductor, is gained by the Mott-Schottky relation, as in the below formulas (1) and (2).

Neglecting the capacitance of the Helmholtz thickness (layer):

$$\frac{1}{C_{SC}^2} = \frac{2}{\epsilon\epsilon_0 e N_D} \left(U - U_{fb} - \frac{kT}{e} \right) \quad (1)$$

$$\frac{1}{C_{SC}^2} = \frac{2}{\epsilon\epsilon_0 e N_A} \left(-U + U_{fb} - \frac{kT}{e} \right) \quad (2)$$

Where, of course, K is the Boltzmann constant ($1.38 \times 10^{-23} \text{JK}^{-1}$), ϵ_0 is the vacuum permittivity ($8.854 \times 10^{-12} \text{Fm}^{-1}$), ϵ represents the dielectric constant of the samples (assumed to be 12 for passive films on IF manganese alloyed steel according to previous studies [28]), e represents the electron charge value ($1.6 \times 10^{-19} \text{C}$), N_D and N_A are carrier concentrations, one N_D is the donor consistency and the other is acceptor density, the absolute temperature follows T and U_{fb} is the potential correlated to the flat band voltage. Respectively, the carrier concentrations are calculated from the slopes of zones of the linear plot.

Figure 3c plots C^2 correlated to the processing potential ($E \& U$), that is, it represents the Mott-Schottky curves of the thin oxide layer formed on IF manganese alloyed steel with different Mn content. These curves clearly reflect the subsistence of three regions on the outermost passive layer formed with different Mn content, where three linear relationships appear with positive and negative slopes between C^2 and E (regions I, II and III). The slopes of the negative and positive sides depicted in the Mott-Schottky plots respectively clarify the p-type and n-type semi-conducting behaviour of the outermost thin protective films. According to previous studies [3], in oxide films which both passively and thermally protect, the heterojunction may comprise inner parts of oxides of other elements, such as

chromium or manganese, with p-type semi-conductivity[29] and an outer field of iron oxide with n-type semi-conductivity[25,30].

Table 2. Fitting parameters for different types of IF manganese alloyed steel with different Mn content in 1.0×10^{-5} mol/L Na_2SO_4 solution

Mn content (wt%)	0.079	0.311	0.556
E_{corr}/V	-0.335	-0.435	-0.318
I_{corr}/Acm^{-2}	2.62×10^{-7}	3.13×10^{-6}	2.18×10^{-6}
$R1/\Omega cm^2$	9.02	16.07	16.56
$R2/\Omega cm^2$	884.4	415.3	92.95
Q/Scm^{-2}	2.58×10^{-3}	/	/
$C1/Fcm^{-2}$	6.21×10^{-4}	3.95×10^{-6}	4.60×10^{-6}
$R3/\Omega cm^2$	33.45	78.91	271.6
$C2/Fcm^{-2}$	1.12×10^{-3}	5.05×10^{-6}	1.77×10^{-5}
$R4/\Omega cm^2$	215.1	514.4	/
$C3/Fcm^{-2}$	/	1.59×10^{-5}	/
$N_p/cm^{-3}(-1V \sim -0.73V)$	1.79×10^{20}	4.90×10^{20}	6.60×10^{20}
$N_{D1}/cm^{-3}(-0.73V \sim -0.5V)$	6.400×10^{20}	7.310×10^{20}	7.365×10^{20}
$N_{D2}/cm^{-3}(-0.5V \sim -0.2V)$	6.799×10^{19}	9.658×10^{19}	1.416×10^{20}

For region I, the negative slopes in the Mott-Schottky curve when the processing potential is under -0.73V clarify that the thin-oxide superficial layers of manganese are expressed as p-type semiconductors, which decreases with increasing Mn content. Also, the results described above agree well with those other researchers obtained by analytical methods[27]. In fact, their work has shown that, formed on the film-electrolyte interface, the outer oxide thickness of iron is much greater than the layer which is mixed with manganese oxide and achieved at the film interface. Mainly, the outer oxide film comprises manganese oxides as shown by XPS; these oxides are considered the final acceptor substance in p-type passive film due to the vacancy, V^{3+}_{Mn} . Based on formula (2), the carrier concentration N_{ps} is calculated. The volatility of acceptor densities N_{ps} greatly influences the electrochemical performance; with their increase, the delivery process of electrons is strengthened, as is the activity of electrochemical reaction. The consequently accelerated dissolution of passive film manifests as reduced stability of the protective passivation layer.

With regard to regions II and III, the positive slope indicated in the Mott-Schottky curves from -0.73 to -0.2V clarifies that the layers of manganese oxide behave like an n-type semiconductor. The passive film generated on IF manganese alloyed steel in 1.0×10^{-5} mol/L Na_2SO_4 solution is primarily composed of Fe_2O_3 , as detected by XPS. Other compounds in the film, such as Fe_2O_3 , perform as an n-type semiconductor, showing that the analysis of the result gained from Mott-Schottky is reasonable. The distinction of positive slopes in the above analysis indicates that carrier concentration transforms with gradual changes of potential. Corrosion resistance takes the reverse relationship with carrier concentration, divided into the donor and acceptor densities (N_D and N_A) of the Fe and Mn oxide layers. Thus, connected with the increase in the donor and acceptor densities of oxide film in the

solution, the existence of decreasing donor vacancies cannot prevent cationic migration and the intrusion of harmful particles. Electrochemical activation improves, and the electrical conductivity of films increases, so the anti-corrosion property decreases. Certain researchers[31] have suspected that the anion consistency of the electric pair layer increases as a result of the increased density of electron acceptors, and so the concentration of chlorine ion in the passive superficial film increases. That enables the chlorine ions to penetrate into the thin passive film. The corrosion phenomenon would then occur more incidentally and maybe more spontaneously, coincident with previous EIS results.

3.3 Effect of Mn content on structure of IF manganese alloyed steel

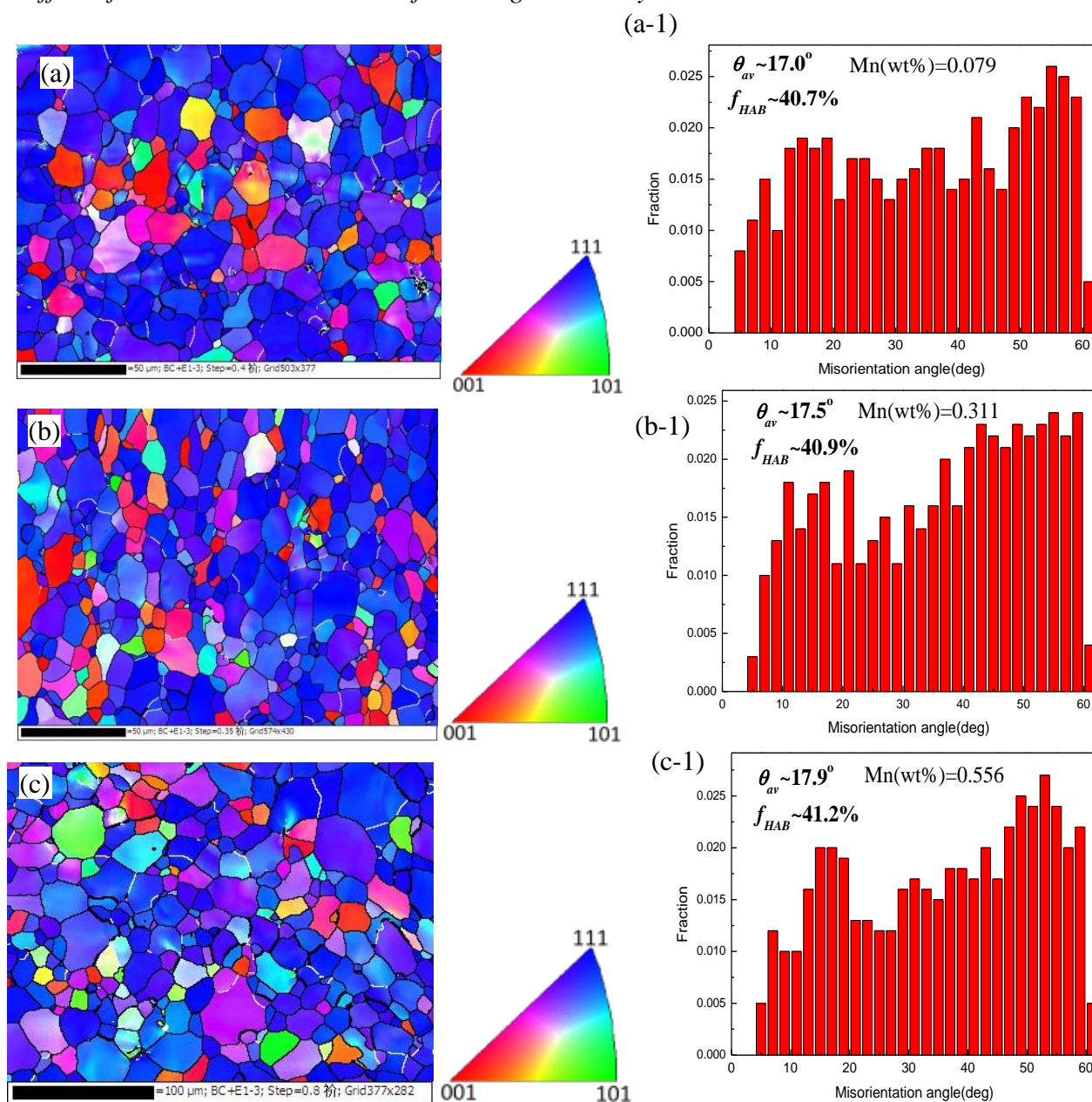


Figure 4. Microstructure changes of IF manganese alloyed steel with different Mn content (wt%) before and after heat treatment: (a)0.079; (b) 0.311; (c)0.556.

Figure 4 displays the electron backscattered diffraction (EBSD) maps and mis-orientation distributions of the present samples with different manganese content. On the EBSD maps, the thin white line indicates small-angle differences in grain-boundary orientation, ranging from 5° to 10° , the bold black line shows orientation differences greater than 10° and less than 15° , and the thin black line manifests large-angle grain boundary distribution differences ranging more than 15° . Many small-angle grain boundaries exist in the grain interior, while a few large-angle grain boundaries extend from the edge of the large grain to the internal part. By comparing the EBSD maps of the partitioned ultrafine grains shown in Fig. 4(a)–(c), the relative fraction ($\sim 11\%$) of the ultrafine grains in Mn content (wt%) of 0.556 was higher than those samples with different Mn content (wt%) at 0.079, and 0.311 ($\sim 9\%$ and $\sim 7\%$, respectively), confirming the significant role of the Mn content on grain refinement of IF manganese alloyed steel.

The evolution of the ultrafine grains was also confirmed by the fraction of high angle boundaries (HABs, f_{HAB}) and average misorientation angle (θ_{av}) as seen from Fig.4(a-1)–(c-1). The f_{HAB} and θ_{av} would tend to increase gradually with increased Mn content (wt%) from 0.079 to 0.556, showing the maximum values of 41.2% and 17.9, respectively, in Mn content (wt%) of 0.556 sample. This indicated the relatively intensive grain refinement in the surface area of the higher Mn content sample. Generally speaking, the proportion of grain-boundary orientations is more decentralized, with an outstanding tendency of grain refinement that represents an active area increase that will change corrosion resistance[31].

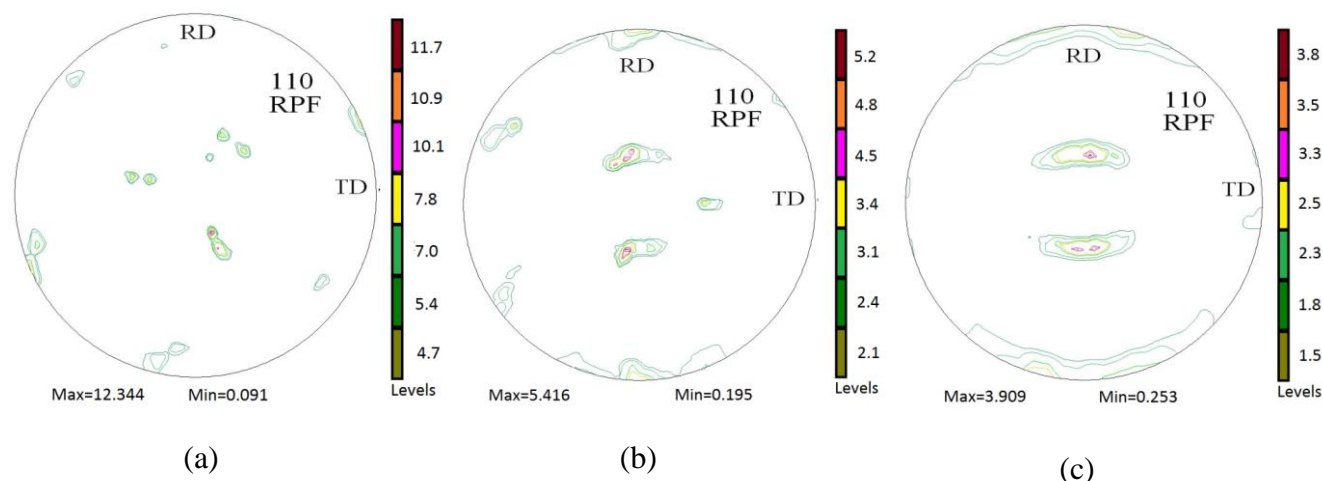
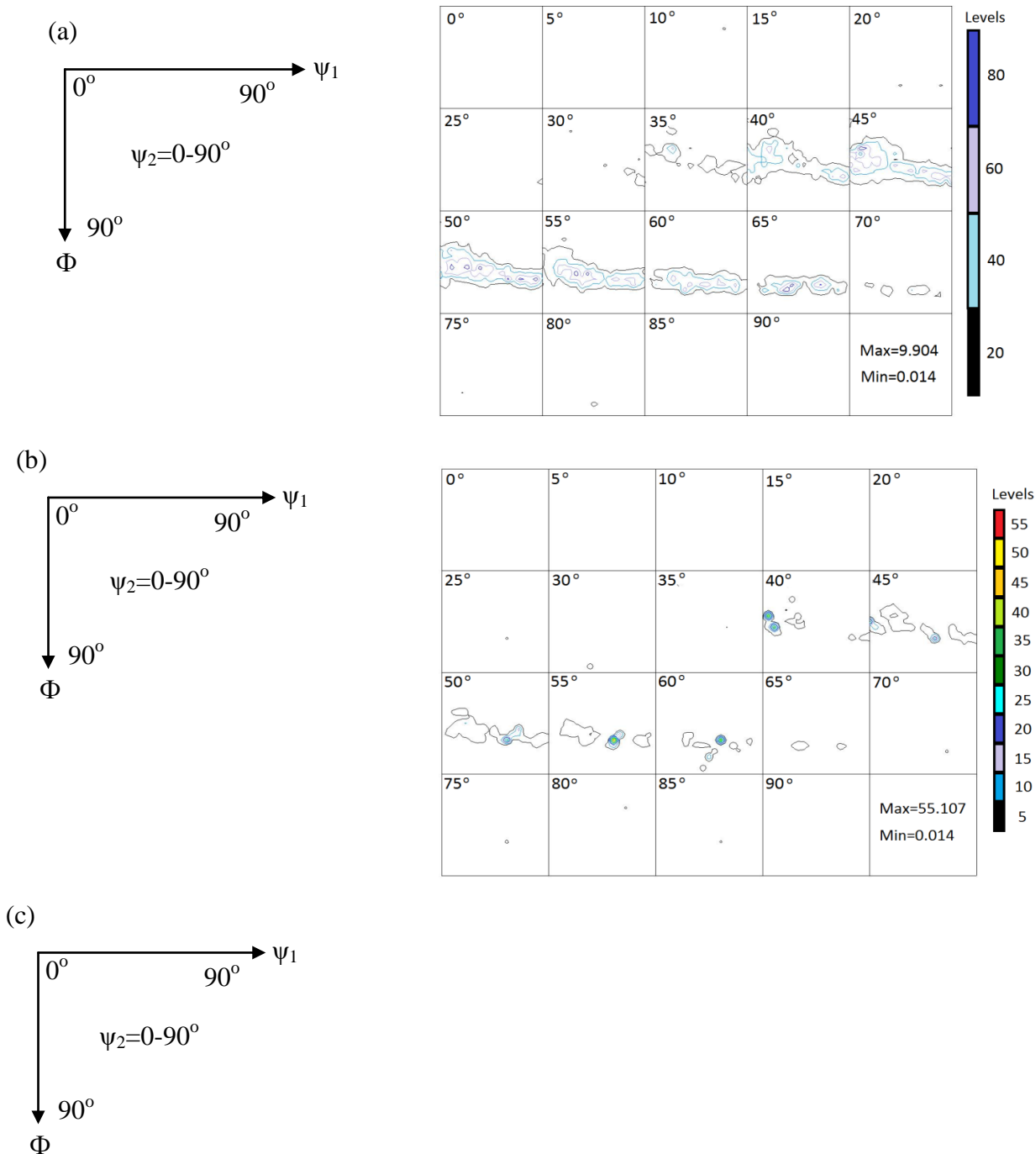


Figure 5. Polar graph of IF manganese alloyed steel with different Mn content (wt%): (a)0.079; (b) 0.311; (c)0.556.

Figure 5 shows the (110) pole plot of IF manganese alloyed steel with different Mn content (wt%) at 0.079, 0.311, and 0.556. Figure 5(a) shows that when the Mn content (wt%) is 0.079, the textural distribution of the (110) poles is relatively diffuse, mainly near the ND pole. Figure 5(b) shows that when the Mn content (wt%) increases to 0.311, the peak of the sample's texture appears near the slope of ND about $\pm 20^\circ$, forming the bimodal base texture considered $\langle 111 \rangle \parallel \text{ND}$ [32]. At the same time, there is a small amount of texture showing near the RD pole, denoted as $\langle 001 \rangle // \text{RD}$. Figure 5(c)

indicates that the textural strength of the bimodal base surface increases significantly when the Mn content (wt%) reaches 0.556. In this case, the texture concentrated at the RD pole tends to move to the TD pole, ranging about $\pm 15^\circ$ to 30° from the vicinity of the RD pole. A small amount of $\langle 001 \rangle // \text{RD}$ texture is also transformed into $\langle 101 \rangle // \text{RD}$ texture. These results show that with increasing Mn content, the texture of the sample gradually stabilizes, both at the RD pole and in the preferred orientation; namely, the bimodal texture near the ND pole gradually increases.



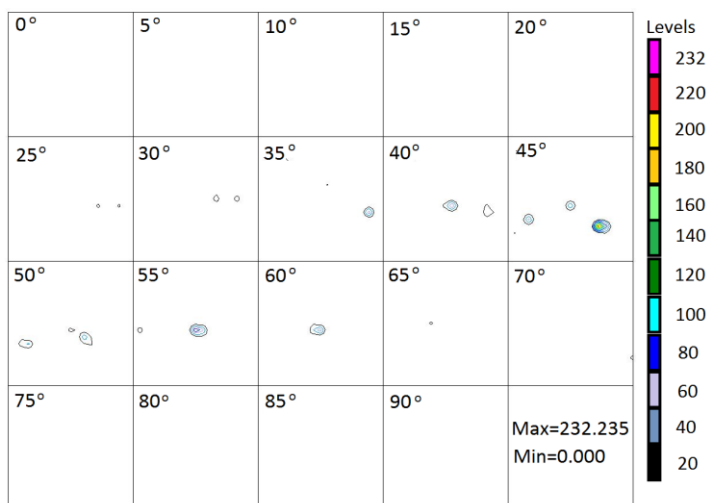


Figure 6. ODF sections of IF manganese alloyed steel with different Mn content (wt%) : (a) 0.079; (b) 0.311; (c)0.556.

Overall, then, according to the polar graph of IF manganese alloyed steel with different Mn content, the proportions increase of Mn or Fe oxides' precipitates. Preliminarily, the preferred orientation appears more clearly. In other words, Mn oxides present more distinctly in the normal direction $\langle 111 \rangle // \text{ND}$. In the direction of the thickness of the passive film, the Mn precipitates appear enriched, which interrupts the integrality of the oxide films. This theory accords with the microstructural changes identified after heat treatment as shown in Figure 4.

Figure 6 shows the ODF cross-sections of IF manganese alloyed steel with different Mn content. These data are taken from the results of XRD. The ODF function of the material is calculated statistically. In the figure, ψ_2 is constant, and the interval is 5° . According to the symmetry of the cubic system, take the measure of $\psi_2 = 0 \sim 90^\circ$ and $\Phi = 0 \sim 90^\circ$. The figure shows that the distribution of high-density contours in the samples is fairly concentrated, indicating that the grain orientation of the samples is obvious and has strong texture. The circular texture forms around $\psi_1 = 30^\circ$ and $\Phi = 20^\circ$ from $\psi_2 = 30^\circ$ to 45° , with gradually increasing density. The polarized density gradually decreases, disappearing completely from $\psi_2 = 45^\circ$ to 60° . At the same time, circular texture forms around $\psi_1 = 75^\circ$ and $\Phi = 75^\circ$ from $\psi_2 = 30^\circ$ to 45° , again with gradually increasing density. The polarized density gradually decreases to disappear completely from $\psi_2 = 45^\circ$ to 60° . As a result, we conclude that $(111)\langle 112 \rangle$ and $(111)\langle 110 \rangle$ are the main textures of the IF manganese alloyed steel samples. With increased Mn content, the texture distribution of IF manganese alloyed steel samples tends to become concentrated, and the density of contour lines increases. For Mn content (wt%) of 0.079, the maximum density is 9.904, which increases to a maximum density of 232.235 at Mn content (wt%) of 0.556.

Figure 7 shows the inverse of the ND IF manganese alloyed steel with different Mn content in the ND direction. Figure 7(a) shows that when the Mn content (wt%) is 0.079, the grain orientation in the plate is mainly $\langle 111 \rangle$ parallel to the rod axis, with a small amount of $\langle 101 \rangle$ parallel to the rod axis. When the Mn content (wt%) is increased to 0.311, as shown in Figure 7(b), the orientation of the crystal grains $\langle 101 \rangle$ parallel to the rod axis converts fully to the $\langle 111 \rangle$ orientation, and the high density exceeds 10. Finally, Figure 7(c) shows that the grain orientation is $\langle 111 \rangle // \text{ND}$ and the

diffusion significantly decreases to form a stable texture with Mn content (wt%) increases to 0.556. We conclude that with increasing Mn content, the high-density contours gradually converge, approaching the $\langle 111 \rangle$ direction, and the dispersion is reduced, which clearly demonstrates a preferred orientation. This conclusion is consistent with the results shown on the polar diagram.

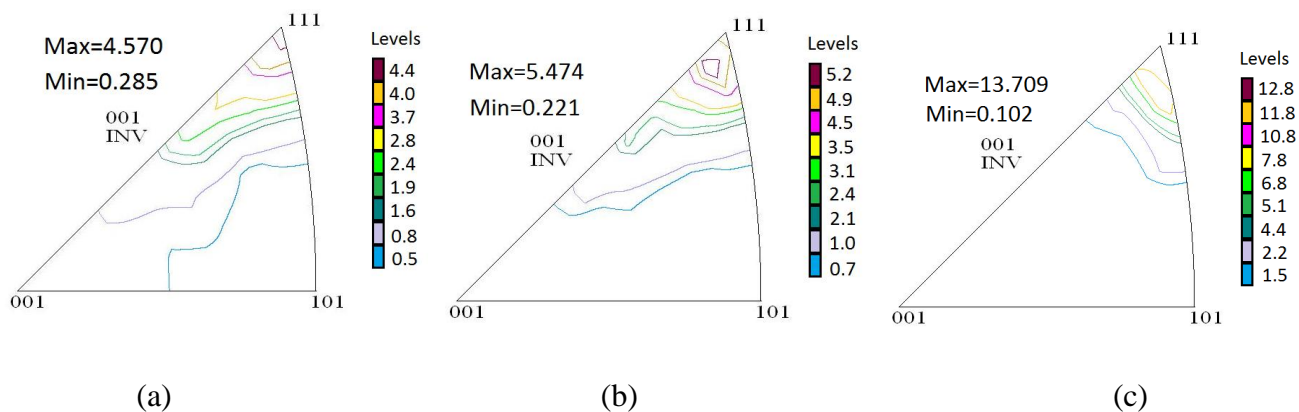


Figure 7. Inverse pole figure on the ND side of IF manganese alloyed steel with different Mn content (wt%): (a)0.079; (b) 0.311; (c)0.556.

Combining the electrical experiments with electron backscattered diffraction analysis, the electrochemical characteristics of the IF manganese alloyed steel show that the anti-corrosion property reduces as Mn content (wt%) increases from 0.079 to 0.556. Given the EBSD results, we conclude that the precipitated phases of Mn greatly influence the corrosive character of IF manganese alloyed steel in the electrolyte 1×10^{-5} mol/L Na_2SO_4 , for various reasons. First, during the precipitation of Mn oxides, the potential difference among Mn oxides and other precipitates will increase, elevating the electrochemical activity of the outer oxide film layer. Meanwhile, along with the enrichment of Mn precipitates, the completeness of the oxide film on IF manganese alloyed steel decreases. Meanwhile, the proportion of grain boundary orientation is more decentralized, and the apparently outstanding tendency of grain refinement represents that increase in active area. All of these phenomenon will result in weakened corrosion resistance with increasing Mn content (wt%) from 0.079 to 0.556. Therefore, the formation of oxide film, including manganese oxide, is closely related to the strain and crystallographic texture of IF manganese alloyed steel.

4. CONCLUSION

This work has made clear the influence of Mn content on corrosion resistance of the outermost thin protective films on IF manganese alloyed steel. Increasing Mn content leads to higher Mn content in the oxide film after annealing, mainly in the form of Mn oxides. In addition, the oxides of other elements (Si and Fe) tend to hold steady with increasing Mn content.

According to the Mott-Schottky curves, alongside increased Mn content, the donor and acceptor densities of oxide film in the solution both increase, as will the potential difference between Mn oxides and the other precipitates, elevating the electrochemical activity of the oxide film's outer

layer. With improved electrochemical activation, the anti-corrosion properties diminish. Meanwhile, Mn oxides make the iron oxide film discontinuous, meaning the corrosion resistance of the IF manganese alloyed steel decreases with increasing Mn oxide in the oxide film.

At the same time, with augmented Mn content, the samples' crystal oriented distribution become clearly concentrated, with the volume fraction of {111} // ND texture increasing and the (111) <112> and (111) <110> textures enhanced. The proportion of grain-boundary orientations is more decentralized, with an outstanding tendency of grain refinement that represents an active area increase that will weaken IF manganese alloyed steel's corrosion resistance.

ACKNOWLEDGMENTS

This work was supported by the National Natural Science Foundation of China [grant number 51374053] and the Iron and Steel Joint Research Fund of the National Natural Science Foundation and China Baowu Steel Group Corporation Limited [grant number U1760118].

References

1. S.H. Song, Y. Zhao, Y.H. Cui, J.Y. Sun, H. Si and J.Q. Li. *Mater. Lett.* 182 (2016) 328.
2. Y.L. Liang, Z.B. Wang, J. Zhang, J.B. Zhang and K. Lu. *Appl. Surf. Sci.* 385 (2016) 341.
3. N.E. Hakiki. *Corros. Sci.* 53 (2011) 2688.
4. E.M. Mahla and N.A. Nielsen. *J. Electrochem. Soc.* 93 (1948) 378.
5. S. Feliu Jr. and M.L. Pérez-Reventa. *Appl. Surf. Sci.* 229 (2004) 112.
6. L. Freire, M.A. Catarino, M.I. Godinho, M.J. Ferreira, M.G.S. Ferreira, A.M.P. Simões and M.F. Montemor. *Cem. Concr. Compos.* 34 (2012) 1075.
7. J. Jia, W.W. Zhu and X.L. Song. *J. Iron. Steel. Res. Int.* 23 (2016) 692.
8. A.P. de Andrade Manfridini, G.C.D. de Godoy and L. de Arruda Santos. *J. Mater. Sci. Technol.* 6 (2017) 65.
9. D.C. Wen. *Surf. Coat. Technol.* 204 (2009) 511.
10. J.J. Yang, L.X. Fan, J. Jia, R. Wu, X.L. Song and L.L. Jiang. *J. Iron. Steel. Res. Int.* 20 (2013) 47.
11. Y. Hayakawa and J.A. Szpunar. *Acta Mater.* 45 (1997) 1285.
12. S.Q. Cao, J.X. Zhang and J.S. Wu. *Mater. Des.* 27 (2006) 53.
13. Z.F. Zhang and Z.G. Wang. *Prog. Mater. Sci.* 53 (2008) 1025.
14. A.J. Davenport, J.A. Bardwell and C.M. Vitus. *J. Electrochem. Soc.* 142 (1995) 721.
15. C.T. Lee, Z. Qin, M. Odziemkowski and D.W. Shoesmith. *Electrochim. Acta.* 51 (2006) 1558.
16. K. Daub, X. Zhang, J.J. Noël and J.C. Wren. *Corros. Sci.* 53 (2011) 11.
17. R. Sánchez-Tovar, R. Leiva-García and J. García-Antón. *Thin Solid Films.* 576 (2015) 1.
18. X.H. Liu, X.Q. Wu and E.H. Han. *Electrochim. Acta.* 108 (2013) 554.
19. J. Huang, X. Liu, E.H. Han and X. Wu. *Corros. Sci.* 53 (2011) 3254.
20. I. Betova, M. Bojinov, P. Kinnunen, K. Lundgren and T. Saario. *Electrochim. Acta.* 54 (2009) 1056.
21. J. Takahashi, J. Haga, K. Kawakami and K. Ushioda. *Ultramicroscopy.* 159 (2015) 299.
22. X.C. Han, J. Li and K.Y. Zhao. *J. Iron. Steel. Res. Int.* 20(2013)74.
23. A.H. Heuer, H. Kahn and P.M. Natishan. *Electrochim. Acta.* 58 (2011) 157.
24. G. Baril, C. Blanc and N. Pebere. *J. Electrochem. Soc.* 148 (2001) B489.
25. G. Baril and N. Pebere. *Corros. Sci.* 43 (2001) 471.
26. J.B. Lee and S.I. Yon. *Mater. Chem. Phys.* 122 (2010) 194.
27. M. Metikoš-Huković and R. Babić. *Corros. Sci.* 53 (2011) 2176.
28. B. Lovrecek and J. Sefaja. *Electrochim. Acta.* 17 (1972) 1151.

29. N.E. Hakiki, M.F. Montemor, M.G.S. Ferreira and M. Da Cunha Belo. *Corros. Sci.* 42 (2000) 687.
30. M.G.S. Ferreira, N.E. Hakiki, G. Goodlet, S. Faty, A.M.P. Simões and M. Da Cunha Belo. *Electrochim. Acta.* 46 (2001) 3767.
31. Y.B. Wang and J.M. Zeng. *Surf. Coat. Technol.* 245 (2014) 55.
32. L.Y. Zhang and A.B. Ma. *Surf. Coat. Technol.* 232 (2013) 412.
33. A. Chakraborty and R.K. Ray. *Surf. Coat. Technol.* 203 (2009) 1756.

© 2018 The Authors. Published by ESG (www.electrochemsci.org). This article is an open access article distributed under the terms and conditions of the Creative Commons Attribution license (<http://creativecommons.org/licenses/by/4.0/>).